The Spectral Analysis of the Hotspots of Pictor A Radio Galaxy with Chandra

Rameshan Thimmappa

Astronomical Observatory
Jagiellonian University
Krakow

Outline of the talk...

1. Introduction
2. Data analysis
3. Analysis results
4. Conclusion
5. Q & A

Outline

Introduction

- Pictor A Radio Galaxy.

Introduction

- Pictor A Radio Galaxy.
- X-ray Telescopes

Introduction

- Pictor A Radio Galaxy.
- X-ray Telescopes
- Chandra X-ray Observatory

Pictor A Radio Galaxy

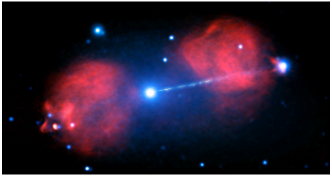

X-ray:NASA/CXC&Radio:CSIRO/ATNF/ATCA

- Pictor A (z=0.035) is FR-II type Broad Line Radio Galaxy.

Pictor A Radio Galaxy

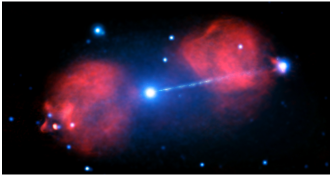

X-ray:NASA/CXC&Radio:CSIRO/ATNF/ATCA

- Pictor A (z=0.035) is FR-II type Broad Line Radio Galaxy.
- Luminosity distance $\Rightarrow$ 154 Mpc.

Pictor A Radio Galaxy

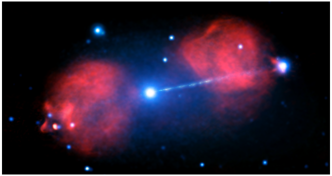

X-ray:NASA/CXC&Radio:CSIRO/ATNF/ATCA

- Pictor A (z=0.035) is FR-II type Broad Line Radio Galaxy.
- Luminosity distance $\Rightarrow$ 154 Mpc.
- There is a well-collimated radio jet passing through prominent radio lobes and terminating into a bright hotspot.

Pictor A Radio Galaxy

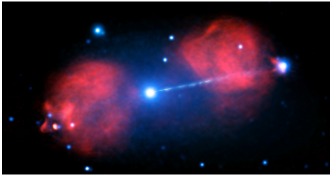

X-ray:NASA/CXC&Radio:CSIRO/ATNF/ATCA

- Pictor A (z=0.035) is FR-II type Broad Line Radio Galaxy.
- Luminosity distance $\Rightarrow$ 154 Mpc.
- There is a well-collimated radio jet passing through prominent radio lobes and terminating into a bright hotspot.
- Total angular extension $\sim 8'$ ($\sim$330 kpc).

Why Pictor A Radio Galaxy

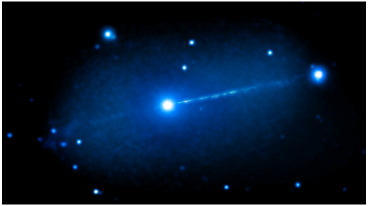

credit: NASA/CXC/Univ of Hertfordshire/ M.Hardcastle et al.,2016

- Pictor A is recognized as an archetypal powerful radio galaxy.

Why Pictor A Radio Galaxy

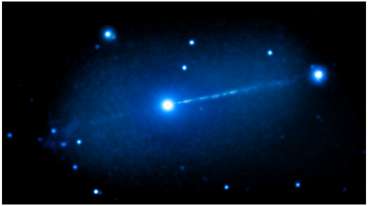

credit: NASA/CXC/Univ of Hertfordshire/ M.Hardcastle et al.,2016

- Pictor A is recognized as an archetypal powerful radio galaxy.
- It became the prime target for detailed multiwavelength investigations in the recent decades, from radio to the γ-ray ranges.

Why Pictor A Radio Galaxy

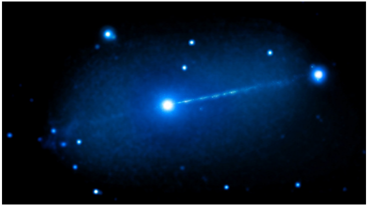

credit: NASA/CXC/Univ of Hertfordshire/ M.Hardcastle et al.,2016

- Pictor A is recognized as an archetypal powerful radio galaxy.
- It became the prime target for detailed multiwavelength investigations in the recent decades, from radio to the γ-ray ranges.
- With Chandra's high spatial resolution and sensitivity, we can resolve in detail the X-ray structure of the core, the jet, the western/eastern hotspots, and the lobes.

Hotspot

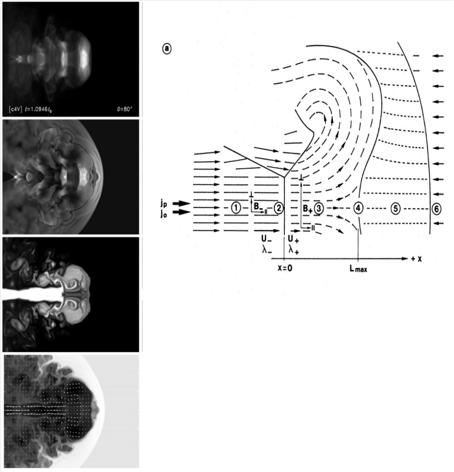

- AGN jets display complex morphology: Knots, Termination hotspot & Radio lobes
- The termination hotspot, marks the location of a strong shock wave, formed where relativistic jet interacts with the intergalactic medium.
- Ultra-relativistic electrons are accelerated efficiently at the front of the termination shock.

Left: Saxton_et al.,2002 & Right: Meisenheimer et al.1989

Hotspot

- Hotspots are known for their broad-band radiation from radio to X-ray bands.
- The two radiative processes at work:
  At low photon energies : synchrotron radiation
  At high photon energies: inverse-Compton radiation
- There are varieties of spectral shapes for the individual hotspots
- W hotspot in Pictor A is particularly prominent in X-rays

What X-rays can tell us?

What X-rays can tell us?

- Thermal emission (= bremsstrahlung + lines) from hot gas: 10^5-10^7 K
  $\Rightarrow$ hot gas is there !

What X-rays can tell us?

- Thermal emission (= bremsstrahlung + lines) from hot gas: 10^5-10^7 K
  $\Rightarrow$ hot gas is there !
- Non-thermal emission: synchrotron, inverse-Comptonization
  $\Rightarrow$ relativistic plasma!

X-ray Telescopes

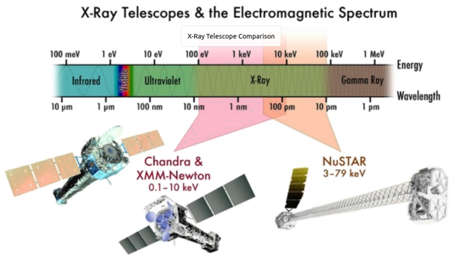

credit: www.nustar.caltech.edu

- Chandra X-ray Observatory

X-ray Telescopes

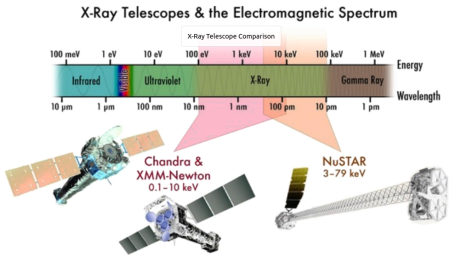

credit: www.nustar.caltech.edu

- Chandra X-ray Observatory
- XMM-Newton

X-ray Telescopes

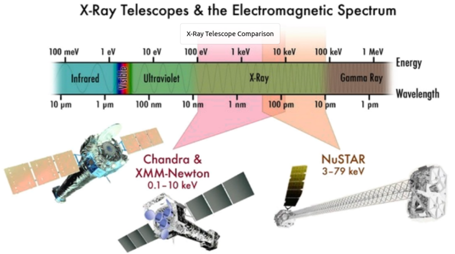

credit: www.nustar.caltech.edu

- Chandra X-ray Observatory
- XMM-Newton
- Nuclear Spectroscopic Telescope Array (NuSTAR)

Chandra X-ray Observatory (CXO)

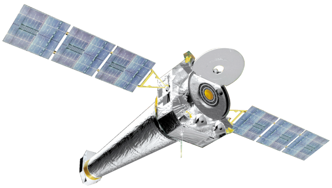

https://science.nasa.gov/toolkits/spacecraft-icons

- Energy Range: 0.1–10 keV
- High spatial resolution $\sim 0.5''$
- High spectral and timing ($\sim$16μs) resolution
- Lifetime: 25-30 years of operation
- A very low background, and so very efficient in detecting low-flux/low-surface brightness sources

Outline

Focusing X-rays

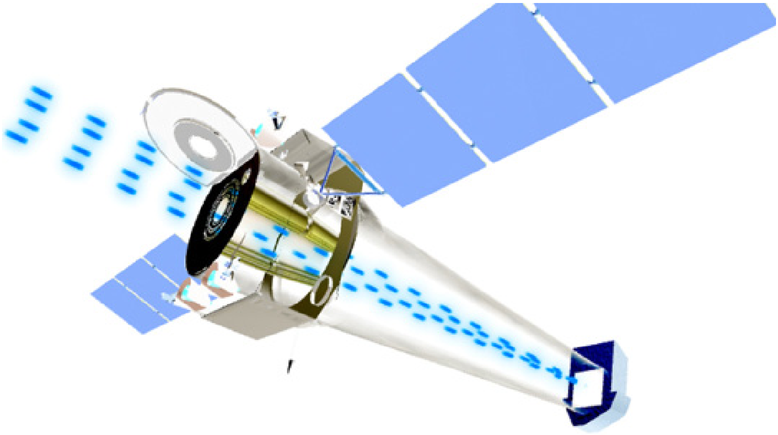

credits: NASA/CXC

Advanced CCD Imaging Spectrometer (ACIS)

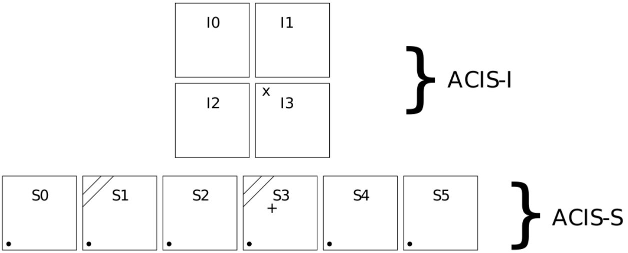

The back illuminated S3 chip offers the best spectral resolution without using a grating. For this reason, many observers choose the back illuminated S3 chip for high resolution imaging over small (few arcminutes) fields. credit: NASA/CXC

Advanced CCD Imaging Spectrometer (ACIS)

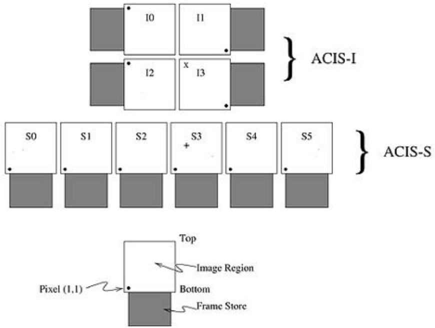

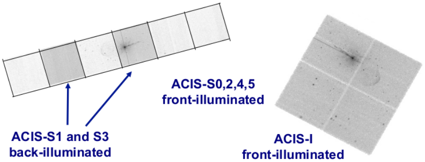

Credits: NASA/CXC

Archival Pictor A data (https://cda.harvard.edu/chaser/)

Obs. ID	Date	Exposure (ks)	Pointing
346	2000-01-18	25.8	Core
3090	2002-09-17	46.4	W hotspot
4369	2002-09-22	49.1	W hotspot
12039	2009-12-07	23.7	Jet
12040	2009-12-09	17.3	Jet
11586	2009-12-12	14.3	Jet
14357	2012-06-17	49.3	Jet
14221	2012-11-06	37.5	Jet
15580	2012-11-08	10.5	Jet
15593	2013-08-23	49.3	Jet
14222	2014-01-17	45.4	Jet
14223	2014-04-21	50.1	Jet
16478	2015-01-09	26.8	Jet
17574	2015-01-10	18.6	Jet

$\sim$ 15 yrs ($\sim$ 464 ks)

Data analysis ⇒ Software packages

- Chandra Interactive Analysis of Observations - CIAO v4.12
- Calibration database - CALDB v4.7.8
- Sherpa v 4.12.0
- ChaRT
- MARX
- SAO ImageDS9 version 8.2

Data analysis ⇒ Chandra Data process

- All ObsID - reprocessed and readout streaks removed.
- Point sources were detected in the field with the `wavdetect` tool and removed for all analyzed ObsIDs.
- Selected photons are in the energy range 0.5–7 keV.
- Spectral fitting - Sherpa package (Freeman et al. 2001).

Point Spread Function (PSF)

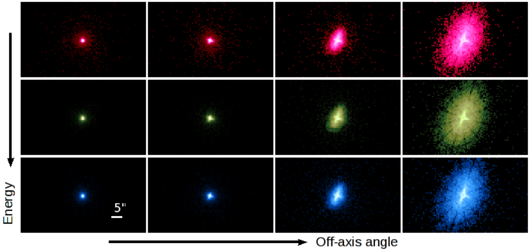

photon energy and off-axis angle

- The shape and size of the PSF varies significantly with source location in the telescope field of view and spectral energy distribution.
- The plot shows simulated PSFs at a set of off-axis angles ($0'$, $2.4'$, $4.7'$, and $9.6'$) and mono-chromatic energies (0.92 keV, 1.56 keV, and 3.8 keV) from the CSC soft, medium, and hard bands.

Focused and analysed regions of Pictor A

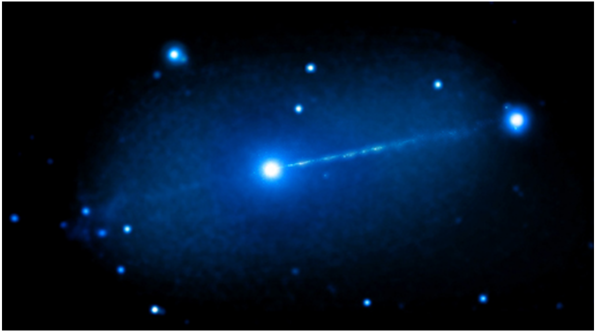

1. W hotspot
2. E hotspot
3. The core

Focused and analysed regions of Pictor A

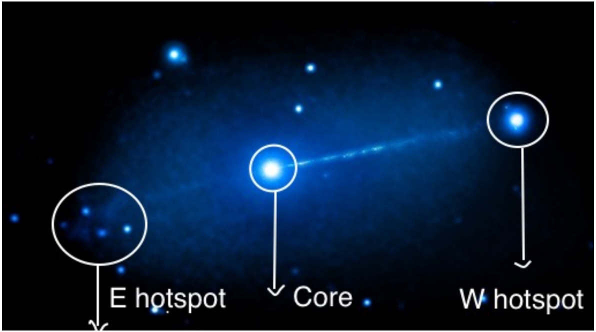

1. W hotspot
2. E hotspot
3. The core

Data analysis ⇒ 1. W hotspot (OBsID 3090)

Spectra extracted for the source (HS) region

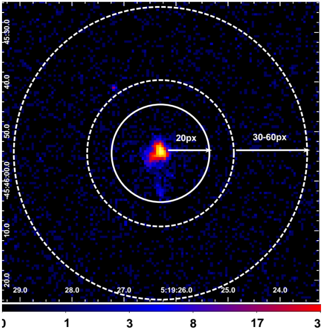

source= 20 px; background=30-60 px

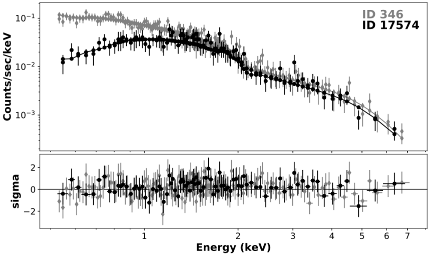

Model: single power-law

Outline

Analysis results ⇒ W hotspot

Observational Data and Spectral Fitting Results

ObsID	Date	MJD	Exposure [ksec]	θ [arcmin]	Γ	red.χ^2	$F_{0.5-7.0\,\mathrm{keV}}$ $[10^{-13}\,\mathrm{erg\,cm^{-2}\,s^{-1}}]$	Counts†
346	2000-01-18	51561	25.8	3.50	2.01 ± 0.05	0.272	5.41 (+0.20 / − 0.45)	3461
3090	2002-09-17	52534	46.4	0.11	1.96 ± 0.03	0.377	5.64 (+0.03 / − 0.20)	5278
4369	2002-09-22	52539	49.1	0.11	1.99 ± 0.03	0.426	5.61 (+0.11 / − 0.15)	5564
12039	2009-12-07	55172	23.7	3.35	1.98 ± 0.06	0.260	5.71 (+0.02 / − 0.10)	2290
12040	2009-12-09	55174	17.3	3.35	2.07 ± 0.08	0.265	5.47 (+0.08 / − 0.25)	1710
11586	2009-12-12	55177	14.3	3.35	2.11 ± 0.09	0.212	5.39 (+0.21 / − 0.40)	1427
14357	2012-06-17	56095	49.3	3.07	2.05 ± 0.05	0.321	5.88 (+0.06 / − 0.14)	3043
14221	2012-11-06	56237	37.5	3.10	2.08 ± 0.05	0.356	5.84 (+0.01 / − 0.11)	3248
15580	2012-11-08	56239	10.5	3.10	2.08 ± 0.14	0.235	5.24 (+0.30 / − 0.21)	935
14222	2014-01-17	56674	45.4	3.30	2.00 ± 0.05	0.329	5.78 (+0.12 / − 0.10)	3428
16478	2015-01-09	57031	26.8	3.32	1.95 ± 0.08	0.232	5.30 (+0.15 / − 0.54)	1657
17574	2015-01-10	57032	18.6	3.32	2.04 ± 0.11	0.209	5.33 (+0.26 / − 0.21)	1187

- ChaRT+MARX (Davis et al.2012) simulations show the data in different aspects of the Chandra PSF.
- We used the Energy-Dependent Sub-pixel Event Repositioning (EDSER) algorithm to adjust chip coordinates and pileup effect also included.

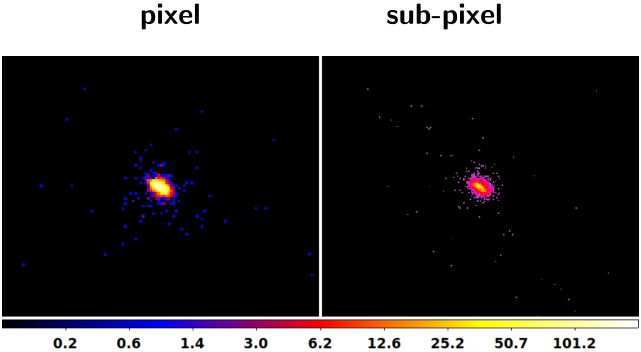

PSF image

Analysis results ⇒ Chandra

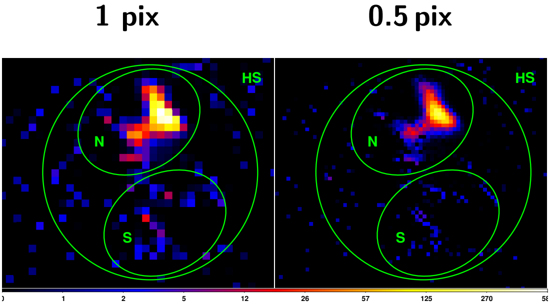

Image Deconvolution

Lucy-Richardson Deconvolution Algorithm (LRDA):

- It is used to remove the effect of the PSF and restore the intrinsic surface brightness distribution of the hotspot.

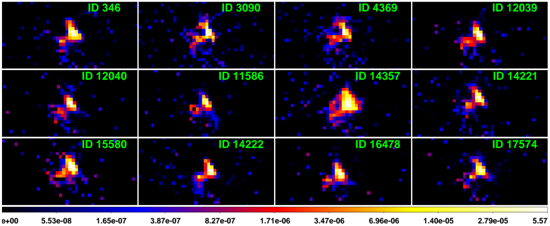

Image Deconvolution (pixel)

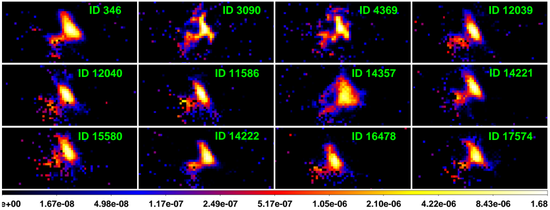

Image Deconvolution (0.5 pix)

Multi-Wavelength Images

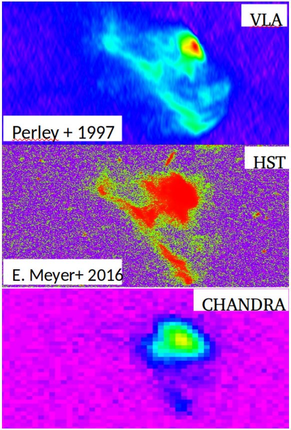

- The WHS of Pictor A is bright in the radio, optical and X-ray bands.
- There are extended structure in the W Hotspot of Pictor A.
  ⇒ Hotspot
  ⇒ Filament
- The hotspot is 10 times brighter than the filament.

VLA: 3.6 cm radio contours are superimposed

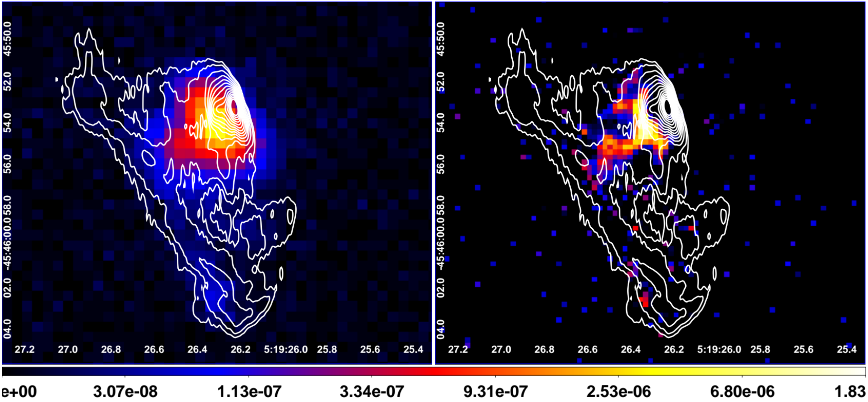

A comparison between the Chandra image of the merging all the analyzed ObsIDs (left panel), and the deconvolved image at 0.5 px resolution for ID 3090, averaged over 100 random realizations of the PSF (right panel).

Chandra: 0.5 px resolution of Pic A for ObsID 3090

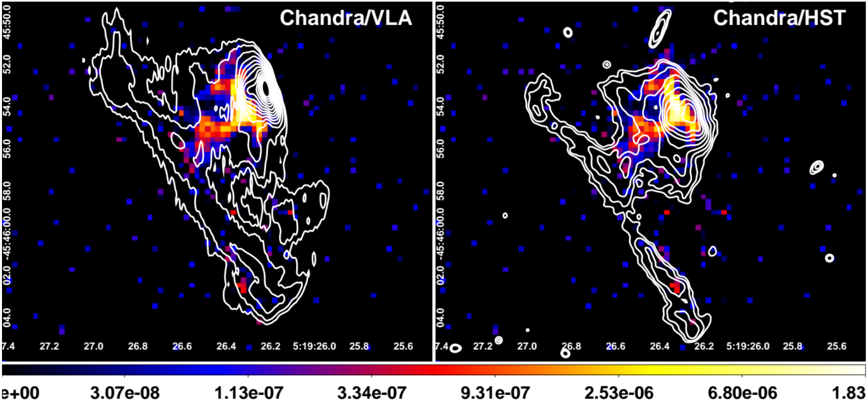

VLA: radio (3.6 cm wavelength, beam size 0.″77x0.″17, position angle -0.4 deg)

HST: optical F606W filter (5918 Å, 90% encircled energy within radius 0.35″) ACS/WFC.

Chandra: 1.0 px resolution image of ObsID 3090

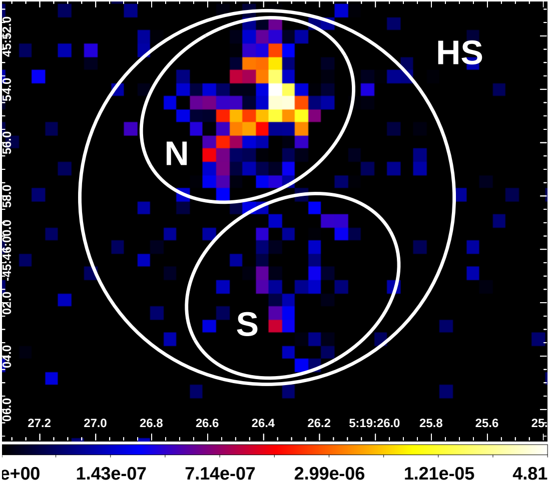

HS - 14 px, N & S - 8.5 px and 6.5 px

Net count rates of the W hotspot (HS) and sub-regions (N,S)

ObsID	MJD	HS (10^{-6} cts s^{-1})	N (10^{-6} cts s^{-1})	S (10^{-6} cts s^{-1})
346	51561	291.3 ± 0.4	283.0 ± 0.5	7.0 ± 0.3
3090	52534	260.1 ± 0.2	251.8 ± 0.3	6.4 ± 0.1
4369	52539	260.4 ± 0.2	251.3 ± 0.4	6.8 ± 0.1
12039	55172	235.5 ± 0.5	228.7 ± 0.7	5.7 ± 0.3
12040	55174	248.0 ± 0.4	241.0 ± 0.6	6.1 ± 0.3
11586	55177	243.9 ± 0.4	238.0 ± 1.0	2.6 ± 0.5
14357	56095	216.1 ± 0.2	210.3 ± 0.4	4.7 ± 0.2
14221	56237	223.5 ± 0.4	217.1 ± 0.5	5.2 ± 0.2
15580	56239	233.1 ± 0.4	228.8 ± 0.7	2.2 ± 0.4
14222	56674	210.8 ± 0.3	203.7 ± 0.4	6.0 ± 0.2
16478	57031	182.2 ± 0.3	176.2 ± 0.5	4.4 ± 0.3
17574	57032	189.3 ± 0.3	183.4 ± 0.4	4.6 ± 0.3

Analysis results ⇒ Chandra (deconvolved images)

Net count rates of the W hotspot (HS)

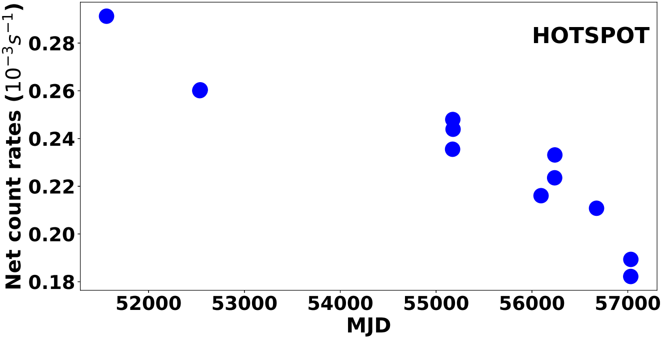

Analysis results ⇒ Chandra

Deconvolution image ⇒ Projection

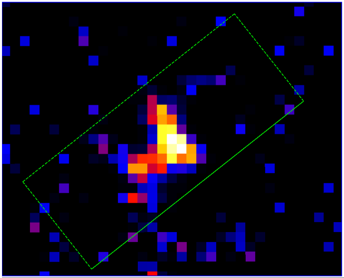

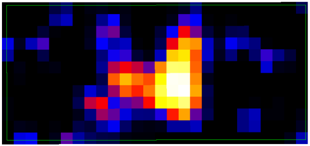

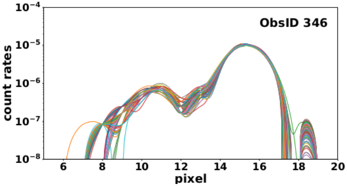

Projection area of hotspot

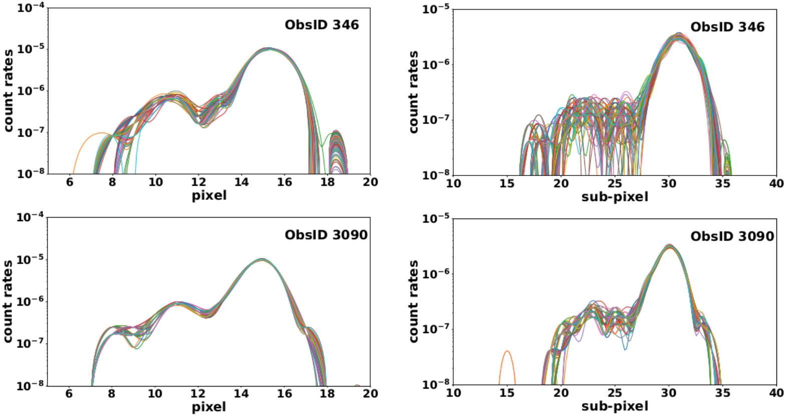

Projection area of hotspot: sub-pixel

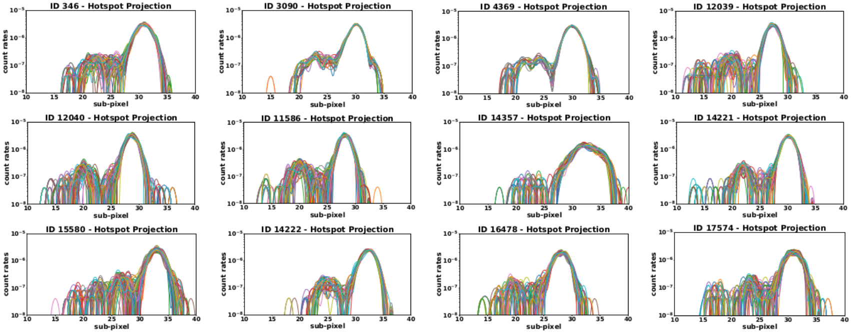

Outline

Conclusion ⇒ W hotspot

- The novelty of the analysis is the detailed PSF simulations and image deconvolution to resolve the X-ray structure of the W hotspot.
  (i) The jet-like feature located in between the radio/optical filament and the termination shock
  (ii) The disk-like feature perpendicular to the jet axis located $\sim 1.''5 \simeq$1kpc upstream the intensity peak of radio hotspot.
- We believe that this disk-like feature - resolved in its longitudinal direction to be $\sim 4''$ $\sim$3 kpc long.
- Its transverse direction with the corresponding scale upper limit of $\sim 0.''25 < 200$ pc marks the position of the reverse shock front in the system.
- Monotonically decreasing count rate on the deconvoled images, about $\sim$ 30% drop over the 15 years (Thimmappa et al. 2020b, ApJ, 903, 109).

Chandra Observational Data

ObsID	Date (YYYY-MM-DD)	MJD	Exposure ks	Detector
346	2000-01-18	51561	25.8	ACIS-23678
12039	2009-12-07	55172	23.7	ACIS-235678
12040	2009-12-09	55174	17.3	ACIS-235678
11586	2009-12-12	55177	14.3	ACIS-235678
14357	2012-06-17	56095	49.3	ACIS-235678
14222	2014-01-17	56674	45.4	ACIS-235678
16478	2015-01-09	57031	26.8	ACIS-235678
17574	2015-01-10	57032	18.6	ACIS-235678

($\sim$ 221 ks)

8 OBsID are merged within the energy range 0.5-7.0 keV.
Point sources are detected with the wavdetect tool.

Exposure-corrected image

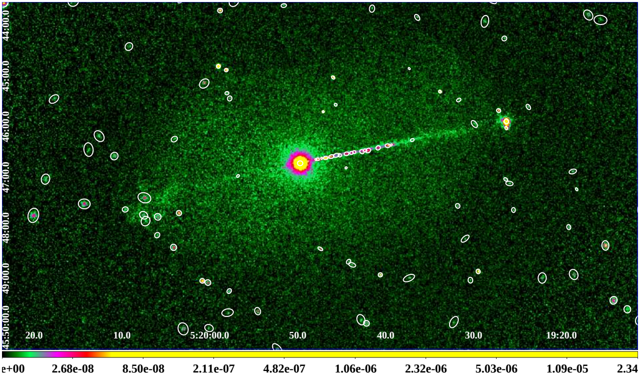

Exposure-corrected merged *Chandra* image + point and compact sources.

VLA Polarized flux and rotation measure map

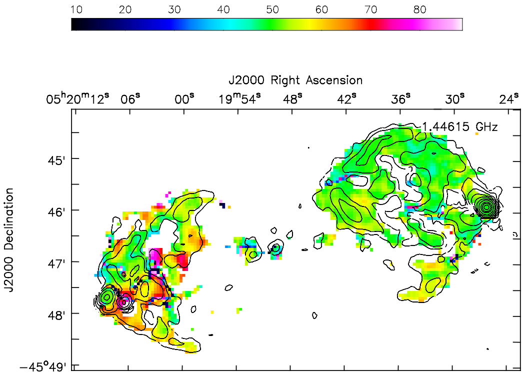

The polarized intensity L-band contours of the source, superimposed on the distribution of RM taken between L- and C- band data, with 10″ resolution. (The radio maps provided by R. Perley; radio images and brightness profiles Prepared by Urszula Pajdosz-Smierciak)

Data analysis ⇒ E hotspot

E hotspot region of Pictor A

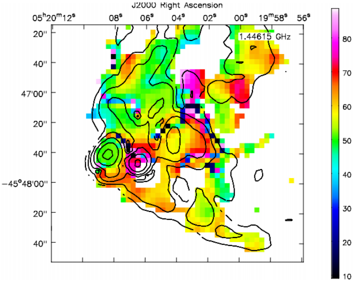

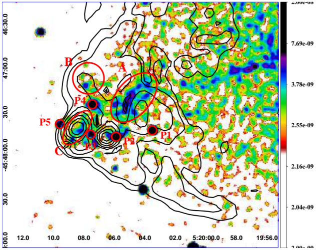

- VLA radio map
  A zoomed view of the RM distribution, with the polarized intensity L band contours superimposed at 10″ resolution.
- Chandra X-ray map
  A zoomed view of the 0.5–7.0 keV Chandra image is smoothed with 3σ Gaussian radius. Selected regions for the Chandra data analysis are labeled and indicated by red contours.

Power-Law model fitting results for the selected regions within the E hotspot

Regions	PhoIndex (Γ)	$F_{0.5-7.0\,keV}$ (10^{-15} erg cm^{-2} s^{-1})	Counts†
src A	$1.70^{+0.23}_{-0.21}$	$21.19^{+3.25}_{-5.33}$	219
src B	$1.89^{+0.55}_{-0.46}$	$4.86^{+2.84}_{-1.34}$	68
src C	$2.17^{+0.62}_{-0.53}$	$5.59^{+1.94}_{-2.22}$	66
src P1	$2.27^{+0.37}_{-0.34}$	$5.07^{+1.94}_{-0.13}$	41
src P2	$2.15^{+0.42}_{-0.39}$	$3.56^{+0.19}_{-1.70}$	27
src P3	$0.43^{+0.71}_{-0.74}$	$4.55^{+0.06}_{-2.99}$	12
src P4	$1.13^{+0.31}_{-0.30}$	$7.85^{+1.11}_{-1.41}$	38
src P5	$1.02^{+0.58}_{-0.57}$	$3.11^{+0.17}_{-1.53}$	12
Background	$0.27^{+0.03}_{-0.03}$	–	–

Analysis results ⇒ ObsID 14357

Power-Law+APEC model fitting results for the source region A

Model[†]	Parameter	Value with 1σ errors	C-stat./DOF
Power-law+APEC	Photon index Γ	$1.27^{+0.27}_{-0.41}$	1074.3/886
	PL normalization	$3.12^{+0.78}_{-0.92} \times 10^{-6}$	
	Temperature kT	$0.27^{+0.14}_{-0.07}$	
	APEC normalization	$5.04^{+4.54}_{-2.63} \times 10^{-6}$	
	Background photon index $\Gamma_{\rm bck}$	$0.27^{+0.08}_{-0.08}$	
	Background normalization	$6.52^{+0.61}_{-0.56} \times 10^{-6}$	

The implied mass of a thermal gas: 3×10^8 $M_\odot$

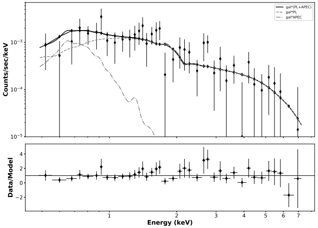

Analysis results ⇒ Confidence contours

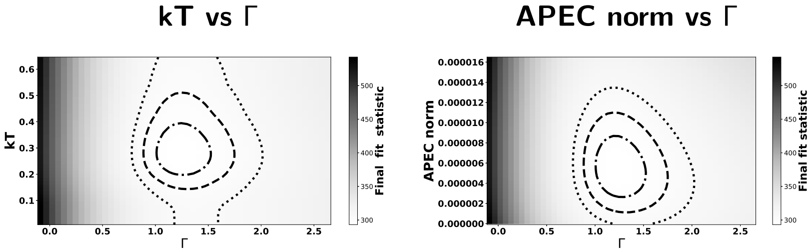

The two-component power-law+APEC model.

E hotspot of Pictor A - X-ray/radio

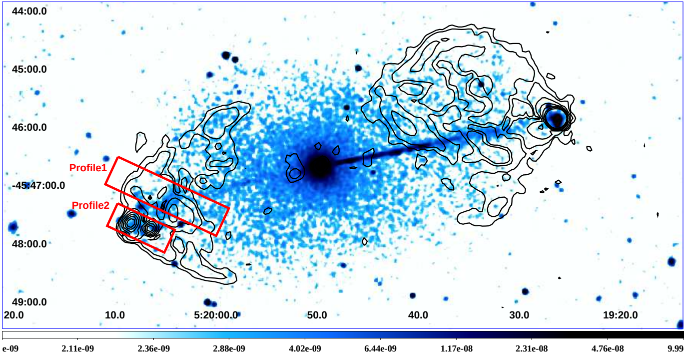

The exposure-corrected 0.5–7.0 keV merged Chandra image of the Pictor A and 1.45 GHz VLA polarized intensity (3σ) contours superimposed (black).

Analysis results ⇒ The Surface Brightness Profile

Pictor A – Profile 1

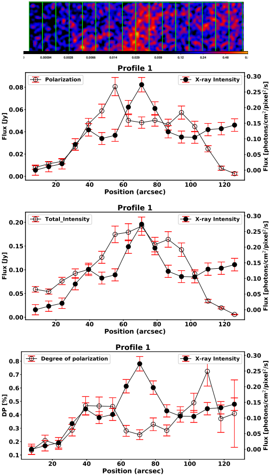

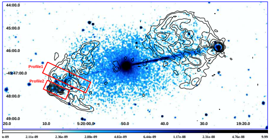

- The Profile1 region, rotated by θ=335°using dmregrid2 tool and is divided into 16 vertical boxes. Energy = 0.5–7.0keV and binsize = 1
- The total and polarized radio flux densities were calculated for the profile1 based on the 1.45 GHz VLA maps.

Analysis results ⇒ The Surface Brightness Profile

Pictor A – Profile 2

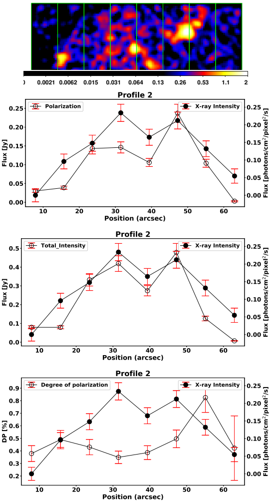

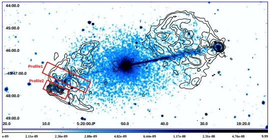

- The Profile1 region, rotated by $\theta = 360^\circ$ using dmregrid2 tool and is divided into 8 vertical boxes. Energy = 0.5–7.0keV and binsize = 1
- The total and polarized radio flux densities were calculated for the profile2 based on the 1.45 GHz VLA maps.

Conclusion

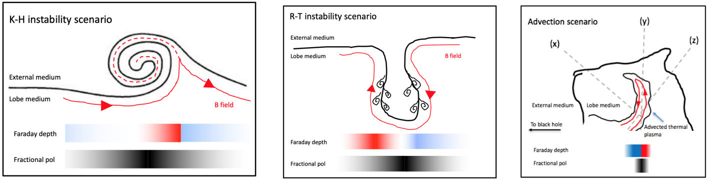

- Anderson et al. 2018: "We argue that the low-polarization patches, along with associated reversals in the line-of-sight magnetic field and other related phenomena, are best explained by the presence of $\sim 1 \times 10^9 M_\odot$ of magnetized thermal plasma in the lobes, structured in shells or filaments,and likely advected from the surrounding ICM."

Conclusion

- The elongated X-ray filament A detected located upstream of the jet termination region, extending for at least 30 kpc (projected).
- Its radiative output within 0.5–7.0 keV is consistent with a pure PL emission with $\Gamma \simeq 1.7 \pm 0.2$, or alternative a combination model of a flat PL model with $\Gamma \simeq 1.3 + 0.3/-0.4$ and a thermal kT $\simeq 0.3$ keV.
- The observed characteristics of the X-ray filament A in the E lobe of Pictor A, is that the degree of the radio linear polarization does increase from about 25% at the filament's axis, up to about 45% at the filament's edges.
- This could indeed be due to the internal depolarization related to the thermal (X-ray emitting) gas present within the filament.
- We observe a clear anti-correlation between the X-ray surface brightness and the polarized radio intensity, as well as a decrease in the radio rotation measure with respect to the surroundings (Thimmappa et al. 2021, accepted in ApJ).

Thank You
For Your Attention

Outline